

2018-09

On the edge of exceptional preservation: insights into the role of redox state in Burgess Shale-type taphonomic windows from the Mural Formation, Alberta, Canada

Sperling, EA

<http://hdl.handle.net/10026.1/11604>

10.1042/ETLS20170163

Emerging Topics in Life Sciences

Portland Press Ltd.

All content in PEARL is protected by copyright law. Author manuscripts are made available in accordance with publisher policies. Please cite only the published version using the details provided on the item record or document. In the absence of an open licence (e.g. Creative Commons), permissions for further reuse of content should be sought from the publisher or author.

1 **On the edge of exceptional preservation: insights into the role of redox state in Burgess**
2 **Shale-type taphonomic windows from the Mural Formation, Alberta, Canada**

3
4
5
6 Erik A. Sperling^{1*}, Uwe Balthasar², Christian B. Skovsted³

7
8 ¹ Department of Geological Sciences, Stanford University, Stanford, CA, USA 94305

9
10 ² School of Geography, Earth and Environmental Sciences, University of Plymouth, PL4 8AA,
11 Plymouth, United Kingdom

12
13 ³ Department of Palaeobiology, Swedish Museum of Natural History, Box 50007, SE-104 05
14 Stockholm, Sweden

15
16
17
18
19
20
21
22
23 * Corresponding author:

24 Dr. Erik A. Sperling
25 Department of Geological Sciences
26 Stanford University
27 Stanford, CA, USA 94305
28 650-736-0852 (v)
29 esper@stanford.edu

30
31
32 **Keywords: Cambrian; Mural Formation; Burgess Shale-type preservation; Oxygen;**
33 **taphonomy; iron reduction**

37 **Abstract**

38

39

40

41

42

43

44

45

46

47

48

49

50

51

52

53

54

55

56

57

58

59

60

Animals originated in the Neoproterozoic and ‘exploded’ into the fossil record in the Cambrian. The Cambrian also represents a high point in the animal fossil record for the preservation of soft tissues that are normally degraded. Specifically, fossils from Burgess Shale-type (BST) preservational windows give paleontologists an unparalleled view into early animal evolution. Why this time interval hosts such exceptional preservation, and why this preservational window declines in the early Paleozoic, have been long-standing questions. Anoxic conditions have been hypothesized to play a role in BST preservation, but recent geochemical investigations of these deposits have reached contradictory results with respect to the redox state of overlying bottom waters. Here, we report a multi-proxy geochemical study of the Lower Cambrian Mural Formation, Alberta, Canada. At the type section, the Mural Formation preserves rare recalcitrant organic tissues in shales that were deposited near storm wave-base (a Tier III deposit; the worst level of soft-tissue preservation). The geochemical signature of this section shows little to no evidence of anoxic conditions, in contrast to published multi-proxy studies of more celebrated Tier I and II deposits. These data help confirm that ‘decay limited’ BST biotas were deposited in more oxygenated conditions, and support a role for anoxic conditions in BST preservation. Finally, we discuss the role of iron reduction in BST preservation, including the formation of iron-rich clays and inducement of sealing seafloor carbonate cements. As oceans and sediment columns became more oxygenated and more sulfidic through the early Paleozoic, these geochemical changes may have helped close the BST taphonomic window.

61

62 **Introduction**

63 The Cambrian radiation of animal life represents the appearance of nearly every major
64 animal phylum in the fossil record within a geologically rapid span of ~25 million years. The
65 rapid increase in animal diversity and disparity is apparent in multiple records including the
66 normal shelly fossil record (e.g. brachiopods, trilobites; (1)), the trace fossil record (2–4),
67 phosphatized small shelly fossils (5–7) and small carbonaceous fossils (SCFs; (8,9)). The most
68 celebrated archive of this event, though, is from Burgess Shale-type (BST) deposits, where
69 primary organic tissues are preserved as thin carbonaceous films (see (10) for definitions).
70 Critically, these lagerstätten preserve the soft parts of animals, and while the communities do not
71 preserve a completely unbiased snapshot of early Cambrian life (for instance, size; (11)), they do
72 provide our best glimpse of early metazoan ecosystems (12–15). Most important, by preserving
73 most or all characters of an organism, fossils from BST biotas have been critical in
74 understanding the polarity and order of morphological character evolution within each individual
75 phylum (16).

76 The question of how organisms can escape the decay process, and why these BST
77 lagerstätten appears to be concentrated in the Cambrian period—even after accounting for factors
78 like rock outcrop area (17,18)—has long intrigued geologists. It was recognized early on that low
79 oxygen levels (or complete anoxia) might play a prominent role in reducing decay. Actualistic
80 decay experiments, however, established that decay under anoxic conditions (at least in the
81 presence of normal marine sulfate levels) can still proceed rapidly (19,20). For soft-bodied
82 deposits in general, then, anoxia mainly serves to 1) prevent scavenging, which would otherwise
83 destroy carcasses (21), and 2) help induce the precipitation of authigenic minerals, which are
84 involved in most exceptionally preserved deposits (22). In the most recent review of BST

85 preservation (10), the window for abundant and exquisite BST fossil preservation is
86 hypothesized to occur in a ‘goldilocks’ zone near where the chemocline (the point in the water
87 column at which no oxygen remains) intersects the seafloor. At seafloor depths well below the
88 chemocline, the setting is ‘supply limited’ in that animals cannot live in anoxic conditions, and
89 carcasses simply cannot be supplied to these preservational settings through transport. Only
90 preservation of nektonic/planktonic organisms falling through the water column could potentially
91 occur. Conversely, at seafloor depths well above the chemocline, the setting is ‘decay limited’
92 (preservation limited) in that aerobic degradation and bioturbating organisms quickly destroy
93 carcasses. Gaines (10) directly related the quality of preservation and species-level diversity of
94 BST biotas to the position of these deposits along the spectrum from ‘supply limited’ to ‘decay
95 limited’. The most spectacular deposits, such as the Burgess Shale and Chengjiang (Tier 1), are
96 hypothesized to occur in the window where there is sufficient transport energy to carry soft-
97 bodied benthic organisms across the chemocline into anoxic waters. Tier II deposits such as
98 Kaili, Marjum and Spence lack sufficient transport energy or have source communities too far
99 up-slope above the chemocline, and so it is dominantly hydrodynamically light organisms (e.g.
100 algae) or dead carcasses that can be carried to the zone of exceptional preservation. Conversely,
101 the labile tissues of organisms living in-situ in these up-slope communities are only rarely
102 preserved due to the prevalence of more oxygenated conditions. Thus at different points along a
103 water-depth transect these Tier II deposits are both supply- and decay-limited. Tier III deposits
104 such as Latham or Indian Springs are hypothesized to have been deposited near storm wave-base
105 in relatively oxygenated conditions, and soft tissues are almost completely decomposed. Or in
106 another sense, only the most recalcitrant tissues are preserved (e.g., (23)). These Tier III sites are
107 consequently the most ‘decay limited’ in this classification scheme.

108 This hypothesized relationship between BST preservation and the chemocline (10) has
109 mainly been developed on the basis of sedimentological and ichnological data (e.g., (24)). To test
110 this framework, in recent years geochemists have applied several tools to the question, most
111 notably iron speciation analysis and the study of redox-sensitive trace metal concentrations. Both
112 of these proxies rely on identifying enrichments of specific phases or elements (that are known to
113 be incorporated into sediments under reducing conditions) relative to average crustal values or
114 empirically determined shale baselines. Iron speciation tracks the ratio of total iron (FeT) to
115 highly reactive iron phases (FeHR; iron in pyrite plus those iron phases reactive to sulfide on
116 early diagenetic timescales, including iron oxides, iron carbonates and magnetite). In the modern
117 ocean, samples deposited beneath an oxygenated water column have $FeHR/FeT < 0.38$ (25,26).
118 Samples deposited beneath an anoxic water column generally have ratios > 0.38 , although rapid
119 deposition, for instance in turbidites, can mute enrichments (the lowest modern anoxic samples
120 have ratios as low as 0.20; (25,27)). Critically, this proxy can also distinguish different types of
121 anoxic water columns: between anoxic and ferruginous water columns (those with free ferrous
122 iron, or more specifically not enough sulfide production to titrate available reactive iron) and
123 anoxic and euxinic water columns (with free sulfide). This is accomplished by examining the
124 proportion of reactive iron that has been pyritized (FeP; represents iron in pyrite). Generally,
125 anoxic samples with $FeP/FeHR > 0.7-0.8$ are interpreted as euxinic, with ratios below this
126 interpreted as ferruginous (26). As discussed below, whether a water column was ferruginous
127 versus euxinic has important implications for interpreting trace metal patterns, and, perhaps, BST
128 preservation itself.

129 Analysis of redox-sensitive trace metal concentrations relies on the observation that these
130 elements (such as molybdenum, uranium, vanadium or chromium) are generally soluble in

131 oxygenated water columns, and become insoluble and form complexes with organic matter,
132 sulfides or other mineral phases upon reduction in suboxic (only trace amounts of oxygen
133 present; ~ 0.1 mL/L) or anoxic (zero oxygen) water columns (28). Such authigenic metal
134 enrichments are identifiable by comparing concentrations in a given shale sample against
135 baselines meant to represent the background detrital input, such as world average shale (29) or
136 average upper continental crust (30). Concentrations above these baselines would point towards
137 authigenic enrichment, and by inference, a reducing water column. Like with iron speciation,
138 rapid deposition will result in less time for authigenic enrichments to accumulate.

139 The sequestration pathways for each element are unique, with different reducing
140 conditions and the presence/absence of sulfide having large effects on the level of enrichment.
141 For instance, sulfide levels $> 11 \mu\text{M}$ are required for the quantitative switch from molybdate
142 anion to tetrathiomolybdate, which increases particle reactivity and hence the removal of Mo
143 from the water column into the sediment (31,32). Vanadium does not require sulfidic conditions
144 for initial reduction, but also undergoes a second reduction step in the presence of significant
145 sulfide levels (33), and the presence of large sedimentary V enrichments may require sulfide.
146 Historically, most of the research on authigenic metal enrichment has focused on modern
147 systems or Mesozoic Ocean Anoxic Events, both of which are characterized by water columns
148 and sediments that were generally sulfidic when anoxic. However, ferruginous conditions are
149 increasingly being identified throughout pre-Mesozoic oceans (26,34–36), and recent debate has
150 focused on expected metal enrichments under such conditions (27,37–40). Although this debate
151 remains open with respect to the exact magnitude of enrichment expected, studies have agreed
152 that redox-sensitive metal enrichments will be relatively muted in ancient ferruginous settings.
153 Further complicating the picture, two elements whose enrichment does not depend on the strict

154 presence of sulfide—vanadium and chromium—are the redox-sensitive metals most influenced
155 by variations in the detrital fraction, making the detection of muted enrichments difficult (28,41).

156

157 **Redox studies of BST deposits**

158 Analyses using iron speciation and some studies of redox-sensitive metal concentrations
159 have provided contrasting interpretations of redox state during deposition of Burgess Shale-type
160 deposits. Consistent with a role for anoxia in the preservational model, iron speciation analyses
161 of the Series 3 Wheeler Shale, Utah, have indicated a mixture of ferruginous and oxic conditions
162 ((35,42); although note that no data to date has been presented in stratigraphic or paleontological
163 context). An iron speciation and trace metal abundance investigation of the Series 2 Chengjiang
164 lagerstätte, South China, revealed euxinic conditions stratigraphically beneath the exceptionally
165 preserved deposits, followed by the development of more ‘equivocal’ conditions in the zone of
166 exceptional preservation (43). Specifically, FeP/FeHR ratios were <0.7 , and FeHR/FeT ratios
167 were between 0.2 and 0.38, which in combination with low Mo concentration and in the context
168 of the turbiditic setting, could indicate either an oxic or ferruginous water column (43,44).

169 Nitrogen isotopes were also investigated in these Chengjiang cores, and showed a more readily
170 interpretable signal. Hammarlund et al. (43) suggested, based on positive nitrogen isotope values,
171 that the water column was strongly denitrifying (similar to the cores of modern Oxygen
172 Minimum Zones; OMZs) above the zone of exceptional preservation. Overall, these data point
173 towards ‘suboxic’ to anoxic (but non-sulfidic) conditions during deposition of the Chengjiang
174 BST deposits. Echoing these results, a detailed multi-proxy study of the Series 2 Sirius Passet
175 deposit in North Greenland reported transiently anoxic (ferruginous) conditions during the
176 interval of highest soft-bodied fossil abundance and diversity (45).

177 In contrast, trace metal data from these and other BST deposits have been interpreted as
178 indicative of oxygenated conditions at the seafloor. Near-crustal levels of redox-sensitive metals
179 (e.g. Mo, U, V, Cr) have been found in the Burgess Shale itself (46), Chengjiang (42,43; though
180 higher abundances were found in the lower Maotianshan Shale), Sirius Passet (47), Emu Bay
181 lagerstätte in South Australia (48), the Rockslide Formation in northwestern Canada (49), the
182 Wheeler and Spence shales in Utah (44) and the Indian Springs lagerstätte, Nevada (50). These
183 relatively low enrichments have generally been interpreted as representing a purely detrital trace
184 metal source and an oxygenated water column. Consequently, it has also been inferred that
185 anoxia did not play a role (or was not required) for BST preservation. In some cases, the
186 robustness of these trace metal signals has been questioned because some deposits (such as the
187 Burgess Shale and Sirius Passet) have experienced considerable metamorphism (24). However,
188 given the consistent and widespread pattern in deposits with lower metamorphic grade, this is
189 probably a primary depositional signature. But while likely primary, the common interpretative
190 paradigm that low redox-sensitive trace metal contents indicate oxygenated conditions (e.g.
191 Jones and Manning ref. (51)) was developed prior to our current understanding that anoxic but
192 non-sulfidic (ferruginous) water columns—with low trace metal enrichments compared to
193 euxinic systems—are common in the geological record. Given this new framework, these
194 published trace metal data provide no evidence for euxinic conditions, but they are also
195 consistent with the muted trace metal enrichments predicted for shale deposited under a
196 ferruginous water column. Thus the role of redox state in BST preservation remains
197 controversial.

198

199 **The Mural Formation: a test case**

200 The Lower Cambrian (Series 2) Mural Formation, exposed in the southern Canadian
201 Cordillera (Fig. 1), offers an opportunity to refine our understanding of the role of redox state in
202 BST preservation. In terms of preservation, the Mural Formation contains elements of BST soft-
203 bodied preservation in one known locality near Mumm Peak (Fig. 1; Fig. 2D, E), but compared
204 to Tier I and II biotas such as the Burgess Shale, Sirius Passet, Emu Bay, or Chengjiang, it is by
205 no means ‘exceptional’ in terms of abundance or preservational fidelity. In essence, it preserves
206 recalcitrant cuticles rather than fine morphologies. Also in contrast to most BST deposits that
207 were deposited well beneath storm wave-base (10), the Mural Formation shows evidence of
208 storm activity in stratigraphic proximity to the beds with exceptional preservation. The Mural
209 Formation therefore represents an end-member of BST preservation: perhaps deposited in
210 slightly shallower water, and with soft-part preservation not seen in standard shelly faunas, but
211 not as exceptional as the deservedly more famous BST deposits. In the classification of Gaines
212 (10) this is a ‘Tier 3’ BST deposit (the worst level of fossil preservation). The goal of this study
213 is to conduct a multi-proxy sedimentary geochemical study of the BST-preservation interval in
214 the Mural Formation—the first such study of a Tier 3 deposit—and compare the results against
215 data obtained from other BST deposits worldwide. Overall this work provides data from a
216 preservational end-member on the role of oxygen in BST taphonomy and an important
217 consistency test of existing hypotheses: if anoxia plays a central role in exceptional BST
218 preservation, we would predict a more oxygenated signal in the Mural Formation than the
219 investigated Tier I and II deposits.

220

221 **Geologic Background**

222 The Mural Formation was deposited during the early Cambrian Sauk transgression on the
223 western Laurentian margin (52,53), and sits above the ~300-1700 meter thick shallow-marine
224 siliciclastics of the McNaughton Formation (54,55). The McNaughton is generally thought to
225 represent the rift-to-post-rift transition on the Laurentian margin (56,57) although continued syn-
226 sedimentary faulting continued through the mid-Cambrian to the north. The Mural Formation is
227 part of a broadly contiguous stratigraphic package spanning the *Nevadella – Bonnia/Olenellus*
228 trilobite zones (Series 2; Waucoban) that stretches from Mexico to Yukon, Canada (52). This
229 package consists of an upper and lower carbonate composed of ooid grainstone shoals and
230 archaeocyath bioherms, separated by a medial shale/siltstone (Fig. 3).

231 The Mural Formation has been the subject of paleontological investigation for more than
232 a century (primarily at its type section near Mumm Peak, Jasper National Park, the focus of study
233 here), and workers have described an abundant shelly fauna including trilobites and obolleid and
234 linguliform brachiopods (58–63). Two known levels have also yielded soft-part preservation
235 (Fig. 3), the ‘*Lingulosacculus* quarry’ that preserves soft-shelled brachiopods (64) (Fig. 2E), and
236 the ‘waterfall quarry’ level which contains as-yet undescribed vetulicolians, palaeoscolecoid
237 worms, and anomalocarid appendages (Fig. 2D). These soft-bodied preservation levels are
238 located in grey, laminated shales between packages of shale containing beds and lenses of
239 detrital carbonates, sometimes comprised of fossil hash. Whether these storm beds represent a
240 shallowing into storm wave base during sea-level change (i.e. parasequences) or occasional
241 storm beds at a constant depth could not be determined, but in either case this represents a
242 proximity to wave base not seen in Type I and II BST deposits (10). The Mural Formation does
243 not display bioturbation through the medial shale.

244

245 **Materials and Methods**

246 27 shale samples were collected from the Mural Formation, all from the medial shale at
247 the type section, and crushed in a tungsten carbide shatterbox. Total organic carbon (TOC)
248 weight percent was analyzed on decalcified residue on a Carlo-Erba NA 1500 Elemental
249 Analyzer. Weight percent iron in pyrite (FeP) was quantified using the chromium reducible
250 sulfur method of Canfield et al. (65), and iron present in iron oxides, iron carbonates and
251 magnetite was quantified using the sequential extraction method of Poulton and Canfield (66).
252 Precision estimates for these methods can be found in the supplementary materials of (35,40).
253 Major, minor and trace element concentrations were analyzed by Bureau Veritas, Ltd., using
254 ICP-MS/ICP-OES following multi-acid digestion. Aliquots of the USGS shale standards SBC-1
255 and SGR-1 were sent blind along with samples, and results were consistent with published
256 values.

257

258 **Results and discussion**

259 All geochemical results are plotted on Figure 3 and reported in the Supplementary
260 Information. Total organic carbon (TOC) weight percents in the Mural Formation are relatively
261 low, at 0.14 ± 0.03 (one standard deviation). This probably rules out very high original
262 sedimentary TOC values (as this signature can be retained even in the face of metamorphism,
263 e.g., (67), but as these are outcrop samples from a region that has experienced prehnite-
264 pumpellyite grade (CAI of 3-5) metamorphism (68), the original TOC-richness is unknown and
265 certainly higher. Redox-sensitive trace metal contents are uniformly low and around
266 crustal/average shale values. Specifically, Mo contents are all < 1 ppm, U contents are 2.6 ± 0.4
267 ppm, and V contents are 88 ± 8 ppm. As aluminum, a conservative tracer of detrital input, is also

268 near or even slightly elevated compared to average shale values (9.4 ± 0.5 weight percent), the
269 low redox-sensitive trace metal contents in the Mural cannot be explained by dilution by
270 carbonates or other non-clastic material. Trace metal data are plotted in Figure 3 as Enrichment
271 Factors (EF), which is a method of accounting for the expected detrital metal input based on
272 observed levels of a biogeochemically conservative element such as aluminum (discussed in
273 (28)). Values $\gg 1$ would indicate authigenic enrichment (due to reducing conditions). Values
274 around 1 generally indicate the operation of purely detrital processes and oxic conditions,
275 however since there is so much possible variability in detrital input (41), and substantial
276 authigenic metal enrichments might also not develop during rapid sedimentation, recognizing
277 whether there have actually been slight enrichments or depletions is difficult to tell. The Mural
278 Formation data unfortunately falls in this zone. Thus, like many other BST deposits investigated
279 to date, the Mural Formation trace metal data rule out euxinic conditions but are consistent with
280 either an oxic (no enrichment) or ferruginous (possibly muted enrichment) water column during
281 deposition.

282 The iron geochemistry of the Mural Formation, though, differs from that of investigated
283 BST deposits. FeHR/FeT values are low (0.17 ± 0.04), with all of the values being well below
284 the 0.38 ratio usually taken as indicative of an anoxic water column. The most straightforward
285 explanation of these data is oxic deposition. However, it has been recognized that 1)
286 fingerprinting anoxia is generally more straightforward than oxic conditions (37,69) and 2) there
287 are a number of factors that can result in low FeHR enrichment (rapid deposition and source area
288 effects) or drive FeHR/FeT values lower (metamorphism). Regarding rapid deposition, the
289 medial shale does not have consistent sedimentological indicators of such processes, although it
290 should be noted that obvious sedimentary structures are difficult to see in outcrop. There is

291 evidence for event-driven sedimentation in a relatively thick sandstone marker bed right above
292 the exceptionally preserved interval. Considering that almost all BST deposits involve event-
293 based sedimentation (10), more detailed sedimentological and petrographic study of the Mural
294 Formation may reveal additional evidence of these processes. Nonetheless, the observed
295 FeHR/FeT values are still generally lower than the lowest 0.2 ratio recognized in the modern
296 ocean for anoxic turbidites (27), suggesting a most parsimonious interpretation of oxic
297 conditions even with respect to this caveat. Second, in some cases there may not be an
298 appropriate source of detrital iron available to be shuttled into the anoxic basin, and it is this
299 shuttle that ultimately generates the iron enrichments this proxy targets (discussed in (69)).
300 However, such settings are relatively rare, and stratigraphically underlying anoxic
301 Neoproterozoic strata exhibit obvious iron enrichments (36). Perhaps the most important
302 consideration for the Mural is that highly reactive iron can be converted to poorly reactive iron
303 during metamorphism, removing the evidence for anoxic sedimentation ((26,70). Fortunately,
304 total iron (relative to aluminum) is also generally enriched by the iron shuttle under anoxic water
305 columns (71,72), and this ratio is not as strongly affected by metamorphism. With the exception
306 of one sample (interestingly, at the level of the *Lingulosacculus* quarry; Fig. 3), the Fe/Al values
307 (0.48 ± 0.11) are exactly within the range expected of oxic sediments (72). In summary, although
308 we cannot unambiguously rule out anoxic conditions, we can state 1) the only possible anoxic
309 signal—in just one of multiple proxies—occurs at one of the soft-bodied preservation levels, and
310 2) all other available evidence points towards the presence of at least some oxygen in the water
311 column (or more precisely, provides no evidence for anoxia).

312 The Mural Formation thus preserves elements of BST biotas and has no evidence for
313 anoxia. Although seemingly paradoxical, we argue this provides strong evidence for the role of

314 anoxic or periodically anoxic conditions in BST preservation. Put simply, the preservation in the
315 Mural Formation is nowhere near that in the celebrated BST deposits. There is no exquisite,
316 high-fidelity preservation of nervous systems, eyes, gut details, gills, etc. as in other deposits
317 (73–76). The fossils preserved in the Mural Formation at Mumm Peak are the recalcitrant end-
318 members of BST preservation: soft-shelled brachiopods (64), anomalocarid appendages, etc.
319 Exceptionally preserved fossils in the Mural Formation are also rare and low-diversity; despite
320 extensive quarrying during our fieldwork, we did not uncover new taxa that had not been found
321 by previous field parties. Core

322 When comparing between BST deposits, it is worth noting that the overall differences in
323 redox state may have been slight. For instance, the Mural is not extensively burrowed,
324 suggesting the water column was not fully oxygenated. And some of the other more spectacular
325 BST deposits may have been deposited in conditions that rapidly alternated between dysoxic and
326 anoxic/ferruginous conditions, with the chemocline established perhaps only slight above the
327 sediment-water interface (24). However, even considering the known difficulty of tracking low-
328 oxygen conditions with available geochemical proxies (77), it is apparent that exceptional BST
329 deposits (Tier 1 and 2) have a much greater prevalence of anoxic iron speciation signatures
330 and/or total iron enrichments, minor but observable trace metal enrichments, and positive
331 nitrogen isotope values (35,42,43,45) than the Mural Formation. In other words, there is now
332 geochemical evidence suggesting both the Mural Formation and the transition between the upper
333 Maotianshan Shale and Yuanshan Member 3 in the Chengjiang deposit (43) were more
334 oxygenated and ‘decay limited’ than Tier I and II deposits. This confirms previous analyses
335 based on detailed sedimentological and ichnological studies that preservation in BST deposits
336 was facilitated by anoxic conditions (24).

337

338 **Towards a refined geochemical model**

339 Moving forward, it is clear that anoxia was likely involved in preserving BST fossils, but
340 it is also clear from both sedimentological/ichnological approaches (24,78,79) and multi-proxy
341 geochemical studies (43,45) that these deposits were near the edge of the chemocline, with often-
342 times rapid fluctuations into low-oxygen (suboxic/dysoxic) conditions. Tracking low oxygen
343 levels is difficult with our current geochemical toolkit (77), and further, the
344 ecological/oceanographic timescales that matter for organismal habitat viability and fossil
345 preservation often differ from the integrated longer-term geochemical signals studied in hand
346 samples collected by geochemists (27). Indeed, no published multi-proxy BST dataset is
347 completely unambiguous; such ambiguity may actually be a hallmark of very low-oxygen or
348 fluctuating oxic/anoxic systems. In light of this, further gains in understanding of the role of
349 redox conditions will require new approaches. These may include increased efforts to obtain
350 unoxidized drill cores (packsack or ‘winky’ drills may offer an alternative to a full drill rig; e.g.,
351 (80)), and moving from standard bulk-rock geochemistry (such as in this study) to increased
352 micron- and phase-specific interrogation of the geochemical signal, especially in more
353 metamorphosed deposits. Shale-based proxies that can unambiguously resolve oxygenated
354 conditions would also be a major step forward.

355 Most important, geochemical studies should strive towards a multi-proxy approach
356 incorporating as many sources of data as possible, but especially pairing redox-sensitive trace
357 metal analysis with iron speciation. The recognition that water columns were commonly
358 ferruginous (non-euxinic) during this time interval will often make interpretation of trace metal
359 data more difficult. Low Mo abundances are helpful in ruling out fully euxinic water columns

360 (81,82), but in the absence of iron speciation data (the best available method for fingerprinting
361 anoxic but non-euxinic conditions), low concentrations of elements like U, V, and Cr are
362 inconclusive as they could indicate either oxic or ferruginous conditions. Like the Mural
363 Formation, some other 'Tier 3' lagerstätte such as Indian Springs might have been deposited
364 under an oxic water column (50), but this cannot be determined from trace metal data alone. A
365 further issue lies in choosing baseline values. Many studies compare redox-sensitive data to the
366 interpretive scheme of Jones and Manning (51). This study was groundbreaking in its time
367 (especially the cross-validation approach), but current consensus is that the scheme is optimistic
368 in its true ability to detect such subtle redox shifts. Redox-sensitive trace metal behavior in
369 sediments and the water column is complicated, and many of the Jones and Manning proxies
370 (e.g. $V/(V + Ni)$, Ni/Co or V/Cr) take two elements, each with incompletely understood redox
371 properties and perhaps different detrital influences, and combine them together. The sum here is
372 likely less than the parts. In light of this, we propose abandoning the Jones and Manning
373 framework. Nuanced understanding of redox patterns with trace metals remains possible, but this
374 should come through careful comparative study of metal data as single-element enrichment
375 factors or metal/aluminum ratios (while paying heed to possible variation in detrital inputs (41))
376 and with respect to more modern chemical oceanographic studies.

377 How exactly anoxic (or fluctuating anoxic-to-dysoxic) conditions directly impacted BST
378 preservation remains unclear. On the one hand, anoxia is a necessary but insufficient prerequisite
379 for BST preservation by eliminating scavenging (10,19,21). Early calcium carbonate
380 cementation and low oceanic sulfate levels may have been equally important in sealing beds
381 from oxidant delivery and reducing microbial decay (83). Beyond simply considering 'anoxia,' it
382 may actually be the specific flavors of anoxia in the sediment and water column that are

383 important in controlling preservation. Specifically, ‘suboxic’ microbial processes such as iron
384 and manganese reduction dramatically increase alkalinity relative to dissolved inorganic carbon
385 (DIC) and thus raise the calcium carbonate saturation state of porewaters. In contrast, sulfate
386 reduction increases alkalinity ~equal to DIC, and moves saturation state along lines of roughly
387 equal values (Ω) (84). Enhanced iron reduction in Cambrian sediments could therefore have
388 helped induce precipitation of the observed BST seafloor cements critical for ‘sealing’ carcasses
389 in the sediment. It is worth noting here that many, but not all, of the BST cement layers carry a
390 dominant seawater (rather than microbial) carbon isotope signature (83). However a seawater
391 carbon signature can also be found in other carbonate precipitates believed to be triggered by
392 ‘suboxic’ microbial metabolisms (84). Essentially, a dominantly seawater carbon isotope
393 signature does not negate a role for iron reduction, but rather suggests that relatively little
394 microbial respiratory work was required to tip the scales and induce precipitation (84).

395 The fact that there was abundant iron reduction relative to sulfate reduction during early
396 diagenesis in BST deposits has recently been demonstrated by clay mineralogy studies. A recent
397 investigation of 19 Cambrian sedimentary successions on four continents found that BST
398 deposits were highly correlated with the presence of iron-rich clay minerals (berthierine and
399 chamosite) compared to deposits only containing shelly fossils (85). These clays form during
400 early diagenesis by the transformation of detrital clays in the presence of elevated pore-water
401 Fe^{2+} . The exact role of these clays in preservation is unclear, specifically whether they are simply
402 a symptom of some other factor important in BST preservational pathways, or a cause (86,87).
403 Certainly, clays appear to function as anti-microbial agents in decay experiments (88), but the
404 action of iron-rich clays is not significantly different from precursors like kaolinite, and the
405 timescale for the formation of berthierine and chamosite is longer than the timescale required for

406 labile tissue preservation. In any case, considering that pore-water Fe^{2+} will not accumulate in
407 the presence of sulfide (89), it is significant that anoxic Cambrian water columns *and* sediments
408 appear to have had relatively low sulfide-generating potential (35). Thus, a transition in the
409 uppermost sediment column away from extensive iron reduction, and towards sulfate reduction
410 (such as we see in modern OMZs) over the early Phanerozoic may have played multiple
411 geochemical roles in the disappearance of BST preservation. In this view, a transition towards
412 more oxygenated oceans with time may have been important (18), but this alone would be too
413 simplistic; the relative rates of iron versus sulfate reduction matter too. In other words, as oxygen
414 and sulfate levels rose through the Paleozoic (90,91), changes in sediments and water columns
415 towards either more oxic or more sulfidic conditions may have inhibited BST preservational
416 pathways. Most likely, the Burgess Shale-type taphonomic window was propped open by a
417 ‘perfect storm’ of geochemical parameters in the Cambrian ocean (18,83,86,92).

418

419

420 **Summary Points**

- 421 • Poor preservation in Burgess Shale-type deposits is linked to relatively more oxygenated
422 conditions, suggesting anoxia likely played a role in the most exceptionally preserved
423 deposits.
- 424 • The relative dominance of iron reduction compared to sulfate reduction in Cambrian
425 sediments and water columns may have played a key role in factors required for Burgess
426 Shale-type preservation.

427

428

429 **Acknowledgements**

430 We thank Una Farrell, Austin Miller, David Mucciarone and Douglas Turner for lab assistance,
431 Jen Wasylyk at Parks Canada for permitting and logistical help, Jakob Vinther for field
432 assistance, Richard Stockey and Ross Anderson helpful discussion, and Bob Gaines and an
433 anonymous reviewer for formal comments. We thank Yellowhead helicopters for safe flying. We
434 gratefully acknowledge support by the National Geographic Society's Global Exploration Fund -
435 Northern Europe GEFNE113-14.

436

437

438 **Figure 1-** A, B: Geographic position of the Mural Formation section studied here. C: Geological
439 map of the study region, after GSC Map 1499A (93) and modified from (62).

440

441 **Figure 2-** Sedimentology and paleontology of the medial shale/siltstone of the Mural Formation
442 near Mumm Peak. A: Unlike exquisitely preserved Tier I and II BST deposits, the medial shale
443 contains beds and lenses of detrital carbonate with indications of wave or current activity, such
444 as cross beds (arrow). Photo from 107.4 meters; mechanical pencil for scale. B) Shale beds
445 immediately adjacent to beds with current structures have a shelly fauna, with evidence of
446 transport, such as this cluster of trilobite cephalons. Photo from local float at 117 meters,
447 mechanical pencil for scale. C) The lower half of the medial shale also contains laminated grey
448 shale intervals, such as this photo spanning ~114-115 meters, at the 'waterfall quarry' level. 30
449 cm geological hammer for scale. These intervals host rare soft-bodied preservation. D) In-situ
450 fragment of anomalocarid claw (arrow), from 114 meters (within 'waterfall quarry'); diameter of
451 Canadian quarter is 24 mm. E) *Lingulosacculus nuda* (64) with preserved gut trace (arrow), from
452 'Lingulosacculus quarry' at 118.2-118.6 meters. 5 mm scale bar on photo.

453

454 **Figure 3-** Lithostratigraphy and sedimentary geochemistry of the Mural Formation at Mumm
455 Peak. Total measured thickness of the Formation is very similar to that of (59) but the heights of
456 internal units differ slightly. *Nevadella-Bonnia/Olenellus* boundary is resolved to a 3.85m
457 interval between 117.3m and 121.15m. Inset shows expanded stratigraphy of medial
458 shale/siltstone. Geochemical data from left-to-right: 1) The iron speciation proxy (FeHR/FeT).
459 Values above the vertical 0.38 line likely represent deposition under an anoxic water column,
460 based on calibrations from the modern ocean (25). Oxidic samples in the modern fall below this
461 line, but anoxic samples can too, for instance during turbiditic sedimentation. The dashed 0.2 line
462 represents the lowest modern value for an anoxic turbiditic sediment. FeP/FeHR values not
463 graphed as all samples show an oxidic signature; the average is 0.29 ± 0.15 (Supplemental
464 Information) (27). 2) Fe/Al ratio, with shaded blue bar representing the range of values seen in
465 ancient oxidic shale (72). Values above this bar would indicate iron enrichment due to an anoxic
466 water column. 3) Molybdenum Enrichment Factor (EF). 4) Uranium EF. 5) Vanadium EF. For
467 these samples, an Enrichment Factor of 1 represents an aluminum-normalized value equal to
468 upper continental crust (30). Values above 1 indicate enrichment, although recognition of muted
469 enrichments can be difficult due to variations in detrital input (41). Enrichment would be
470 expected under an anoxic water column (28), yet all of these samples are unenriched. McNton. =
471 McNaughton Formation; W. = 'waterfall quarry' level from 112.8-114.9m; L. =
472 'Lingulosacculus quarry' from 118.2-118.6m.

473

474

475 **References**

- 476 1. Erwin DH, Laflamme M, Tweedt SM, Sperling EA, Pisani D, Peterson KJ. The Cambrian
477 conundrum: Early divergence and later ecological success in the early history of animals.
478 Science. 2011;334(6059):1091–7.
- 479 2. Droser ML, Gehling JG, Jensen S. When the worm turned: Concordance of Early Cambrian
480 ichnofabric and trace-fossil record in siliclastic rocks of South Australia. Geology.
481 1999;27:625–8.
- 482 3. Droser ML, Bottjer DJ. Trends in depth and extent of bioturbation in Cambrian carbonate
483 marine environments, western United States. Geology. 1988;16:233–6.
- 484 4. Buatois LA, Mángano MG, Olea RA, Wilson MA. Decoupled evolution of soft and hard
485 substrate communities during the Cambrian Explosion and Great Ordovician
486 Biodiversification Event. Proc Natl Acad Sci. 2016 Jun 21;113(25):6945–8.
- 487 5. Porter SM. Closing the phosphatization window: Testing for the influence of taphonomic
488 megabias on the pattern of small shelly fossil decline. Palaios. 2004;19:178–83.
- 489 6. Smith EF, Macdonald FA, Petach TA, Bold U, Schrag DP. Integrated stratigraphic,
490 geochemical, and paleontological late Ediacaran to early Cambrian records from
491 southwestern Mongolia. GSA Bull. 2016 Mar 1;128(3–4):442–68.
- 492 7. Maloof AC, Porter SM, Moore JL, Dudas FO, Bowring SA, Higgins JA, et al. The earliest
493 Cambrian record of animals and ocean geochemical change. Geol Soc Am Bull.
494 2010;122:1731–74.
- 495 8. Butterfield N, Harvey T. Small carbonaceous fossils (SCFs): A new measure of early
496 Paleozoic paleobiology. Geology. 2012;40(1):71–4.
- 497 9. Harvey THP, Vélez MI, Butterfield NJ. Exceptionally preserved crustaceans from western
498 Canada reveal a cryptic Cambrian radiation. Proc Natl Acad Sci. 2012;109(5):1589–94.
- 499 10. Gaines RR. Burgess Shale-type Preservation and its Distribution in Space and Time.
500 Paleontol Soc Pap. 2014 Oct;20:123–46.
- 501 11. Sperling EA. Tackling the 99%: can we begin to understand the paleoecology of the small
502 and soft-bodied animal majority? In: Bush AM, Pruss SB, Payne JL, editors. Ecosystem
503 paleobiology and geobiology. 2013. p. 77–86.
- 504 12. Conway Morris SC. The community structure of the Middle Cambrian Phyllopod Bed
505 (Burgess Shale). Palaeontology. 1986;29:427–67.
- 506 13. Briggs DEG. Extraordinary fossils reveal the nature of Cambrian life: a commentary on
507 Whittington (1975) ‘The enigmatic animal *Opabinia regalis*, Middle Cambrian, Burgess
508 Shale, British Columbia.’ Phil Trans R Soc B. 2015 Apr 19;370(1666):20140313.
- 509 14. Briggs DEG. Extraordinary Fossils. Am Sci. 1991;79(2):130–41.

- 510 15. Caron J-B, Jackson DA. Paleoeology of the Greater Phyllopod Bed community, Burgess
511 Shale. *Palaeogeogr Palaeoclimatol Palaeoecol.* 2008 Feb 18;258(3):222–56.
- 512 16. Briggs DEG, Fortey RA. Wonderful strife: systematics, stem groups, and the phylogenetic
513 signal of the Cambrian radiation. *Paleobiology.* 2005;31 Supplement:94–112.
- 514 17. Allison PA, Briggs DEG. Exceptional fossil record: Distribution of soft-tissue preservation
515 through the Phanerozoic. *Geology.* 1993 Jun 1;21(6):527–30.
- 516 18. Muscente AD, Schiffbauer JD, Broce J, Laflamme M, O'Donnell K, Boag TH, et al.
517 Exceptionally preserved fossil assemblages through geologic time and space. *Gondwana*
518 *Res.* 2017 Aug 1;48:164–88.
- 519 19. Allison PA. The Role of anoxia in the decay and mineralization of proteinaceous macro-
520 fossils. *Paleobiology.* 1988 Jan 1;14:139–54.
- 521 20. Hammarlund E, Canfield DE, Bengtson S, Leth PM, Schillinger B, Calzada E. The influence
522 of sulfate concentration on soft-tissue decay and preservation. *Palaeontogr Can.*
523 2011;(31):141–56.
- 524 21. Skinner ES. Taphonomy and depositional circumstances of exceptionally preserved fossils
525 from the Kinzers Formation (Cambrian), southeastern Pennsylvania. *Palaeogeogr*
526 *Palaeoclimatol Palaeoecol.* 2005;220(1–2):167–92.
- 527 22. Briggs DEG. The role of decay and mineralization in the preservation of soft-bodied fossils.
528 *Annu Rev Earth Planet Sci.* 2003;31:275–301.
- 529 23. Naimark E, Kalinina M, Boeva N. PERSISTENCE OF EXTERNAL ANATOMY OF
530 SMALL CRUSTACEANS IN A LONG TERM TAPHONOMIC EXPERIMENT.
531 *PALAIOS.* 2018 Apr 10;33(4):154–63.
- 532 24. Gaines RR, Droser ML. The paleoredox setting of Burgess Shale-type deposits. *Palaeogeogr*
533 *Palaeoclimatol Palaeoecol.* 2010 Nov 20;297(3):649–61.
- 534 25. Raiswell R, Canfield DE. Sources of iron for pyrite formation in marine sediments. *Am J*
535 *Sci.* 1998;298:219–45.
- 536 26. Poulton SW, Canfield DE. Ferruginous conditions: A dominant feature of the ocean through
537 Earth's history. *Elements.* 2011;7(2):107–12.
- 538 27. Sperling EA, Carbone C, Strauss JV, Johnston DT, Narbonne GM, Macdonald FA. Oxygen,
539 facies, and secular controls on the appearance of Cryogenian and Ediacaran body and trace
540 fossils in the Mackenzie Mountains of northwestern Canada. *Geol Soc Am Bull.*
541 2016;128:558–75.
- 542 28. Tribouillard N, Algeo TJ, Lyons T, Riboulleau A. Trace metals as paleoredox and
543 paleoproductivity proxies: An update. *Chem Geol.* 2006;232(1):12–32.

- 544 29. Turekian KK, Wedepohl KH. Distribution of the elements in some major units of the earth's
545 crust. *Geol Soc Am Bull.* 1961;72(2):175–92.
- 546 30. McLennan SM. Relationships between the trace element composition of sedimentary rocks
547 and upper continental crust. *Geochem Geophys Geosystems.* 2001 Apr 1;2(4):1021.
- 548 31. Helz GR, Miller CV, Charnock JM, Mosselmans JFW, Patrick RAD, Garner CD, et al.
549 Mechanism of molybdenum removal from the sea and its concentration in black shales:
550 EXAFS evidence. *Geochim Cosmochim Acta.* 1996 Oct 1;60(19):3631–42.
- 551 32. Erickson BE, Helz GR. Molybdenum(VI) speciation in sulfidic waters: Stability and lability
552 of thiomolybdates. *Geochim Cosmochim Acta.* 2000 Apr 1;64:1149–58.
- 553 33. Wanty RB, Goldhaber MB. Thermodynamics and kinetics of reactions involving vanadium
554 in natural systems: Accumulation of vanadium in sedimentary rocks. *Geochim Cosmochim*
555 *Acta.* 1992 Apr 1;56(4):1471–83.
- 556 34. Guilbaud R, Poulton SW, Butterfield NJ, Zhu M, Shields-Zhou GA. A global transition to
557 ferruginous conditions in the early Neoproterozoic oceans. *Nat Geosci.* 2015;8:466–70.
- 558 35. Sperling EA, Wolock CJ, Morgan AS, Gill BC, Kunzmann M, Halverson GP, et al.
559 Statistical analysis of iron geochemical data suggests limited late Proterozoic oxygenation.
560 *Nature.* 2015 Jul 22;523(7561):451–4.
- 561 36. Canfield DE, Poulton SW, Knoll AH, Narbonne GM, Ross G, Goldberg T, et al. Ferruginous
562 conditions dominated later Neoproterozoic deep-water chemistry. *Science.* 2008;321:949–
563 52.
- 564 37. Sperling EA, Rooney AD, Hays L, Sergeev VN, Vorob'eva NG, Sergeeva ND, et al. Redox
565 heterogeneity of subsurface waters in the Mesoproterozoic ocean. *Geobiology.* 2014;12:373–
566 386.
- 567 38. Li C, Planavsky NJ, Love GD, Reinhard CT, Hardisty D, Feng L, et al. Marine redox
568 conditions in the middle Proterozoic ocean and isotopic constraints on authigenic carbonate
569 formation: Insights from the Chuanlinggou Formation, Yanshan Basin, North China.
570 *Geochim Cosmochim Acta.* 2015 Feb 1;150:90–105.
- 571 39. Marz C, Poulton SW, Beckmann B, Kuster K, Wagner T, Kasten S. Redox sensitivity of P
572 cycling during marine black shale formation: Dynamics of sulfidic and anoxic, non-sulfidic
573 bottom waters. *Geochim Cosmochim Acta.* 2008;72:3703–17.
- 574 40. Miller AJ, Strauss JV, Halverson GP, MacDonald FA, Johnston DT, Sperling EA. Tracking
575 the onset of Phanerozoic-style redox-sensitive trace metal enrichments: New results from
576 basal Ediacaran post-glacial strata in NW Canada. *Chem Geol.* 2017 Mar 1;457:24–37.
- 577 41. Cole DB, Zhang S, Planavsky NJ. A new estimate of detrital redox-sensitive metal
578 concentrations and variability in fluxes to marine sediments. *Geochim Cosmochim Acta.*
579 2017 Oct 15;215:337–53.

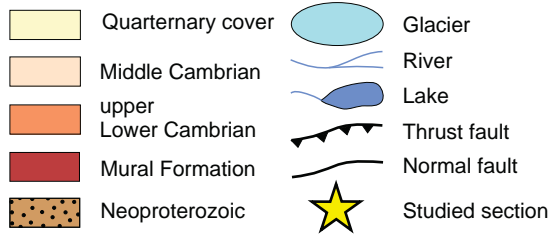
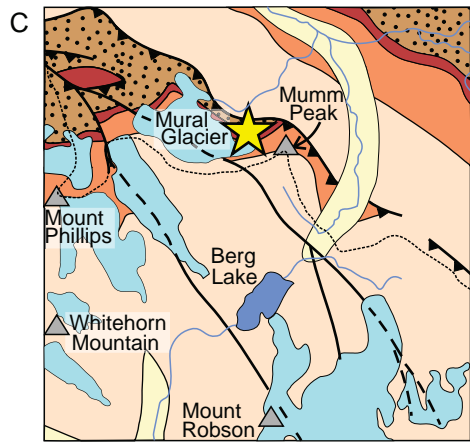
- 580 42. Raiswell R, Canfield DE. The iron biogeochemical cycle past and present. *Geochem*
581 *Perspect.* 2012;1(1):1–322.
- 582 43. Hammarlund EU, Gaines RR, Prokopenko MG, Qi C, Hou X-G, Canfield DE. Early
583 Cambrian oxygen minimum zone-like conditions at Chengjiang. *Earth Planet Sci Lett.* 2017
584 Oct 1;475:160–8.
- 585 44. Kloss TJ, Dornbos SQ, Chen J-Y, McHenry LJ, Marenco PJ. High-resolution geochemical
586 evidence for oxic bottom waters in three Cambrian Burgess Shale-type deposits. *Palaeogeogr*
587 *Palaeoclimatol Palaeoecol.* 2015 Dec 15;440:90–5.
- 588 45. Hammarlund E, Smith, M.P., Rasmussen, J., Nielsen, A., Canfield, D., Harper, D. The Sirius
589 Passet Lagerstätte of North Greenland - a geochemical window on early Cambrian low
590 oxygen environments and ecosystems. *Geobiology.* in review;
- 591 46. Powell WG, Johnston PA, Collom CJ. Geochemical evidence for oxygenated bottom waters
592 during deposition of fossiliferous strata of the Burgess Shale Formation. *Palaeogeogr*
593 *Palaeoclimatol Palaeoecol.* 2003 Dec 5;201(3):249–68.
- 594 47. Boudec AL, Ineson J, Rosing M, Døssing L, Martineau F, Lécuyer C, et al. Geochemistry of
595 the Cambrian Sirius Passet Lagerstätte, Northern Greenland. *Geochem Geophys*
596 *Geosystems.* 2014 Apr 1;15(4):886–904.
- 597 48. McKirdy DM, Hall PA, Nedin C, Halverson GP, Michaelsen BH, Jago JB, et al. Paleoredox
598 status and thermal alteration of the lower Cambrian (Series 2) Emu Bay Shale Lagerstätte,
599 South Australia. *Aust J Earth Sci.* 2011 Apr 1;58(3):259–72.
- 600 49. Kimmig J, Pratt BR. Taphonomy of the middle Cambrian (Drumian) Ravens Throat River
601 Lagerstätte, Rockslide Formation, Mackenzie Mountains, Northwest Territories, Canada.
602 *Lethaia.* 2016 Apr 1;49(2):150–69.
- 603 50. Novek JM, Dornbos SQ, McHenry LJ. Palaeoredox geochemistry and bioturbation levels of
604 the exceptionally preserved early Cambrian Indian Springs biota, Nevada, USA. *Lethaia.*
605 2016 Oct 1;49(4):604–16.
- 606 51. Jones B, Manning DAC. Comparison of geochemical indices used for the interpretation of
607 palaeoredox conditions in ancient mudstones. *Chem Geol.* 1994;111:111–29.
- 608 52. Pope MC, Hollingsworth JS, Dilliard K. Overview of Lower Cambrian mixed carbonate-
609 siliciclastic deposition along the western Laurentian passive margin. In: Derby JR, Fritz RD,
610 Longacre SA, Morgan WA, Sternbach CA, editors. *The great American carbonate bank: The*
611 *geology and economic resources of the Cambrian-Ordovician Suak megasequence of*
612 *Laurentia.* AAPG Memoir; 2012. p. 735–50.
- 613 53. Pyle LJ. Cambrian and Lower Ordovician Suak megasequence of northwestern Canada,
614 northern Rocky Mountains to the Beaufort Sea. In: Derby JR, Fritz RD, Longacre SA,
615 Morgan WA, Stembach CA, editors. *The great American carbonate bank: The geology and*

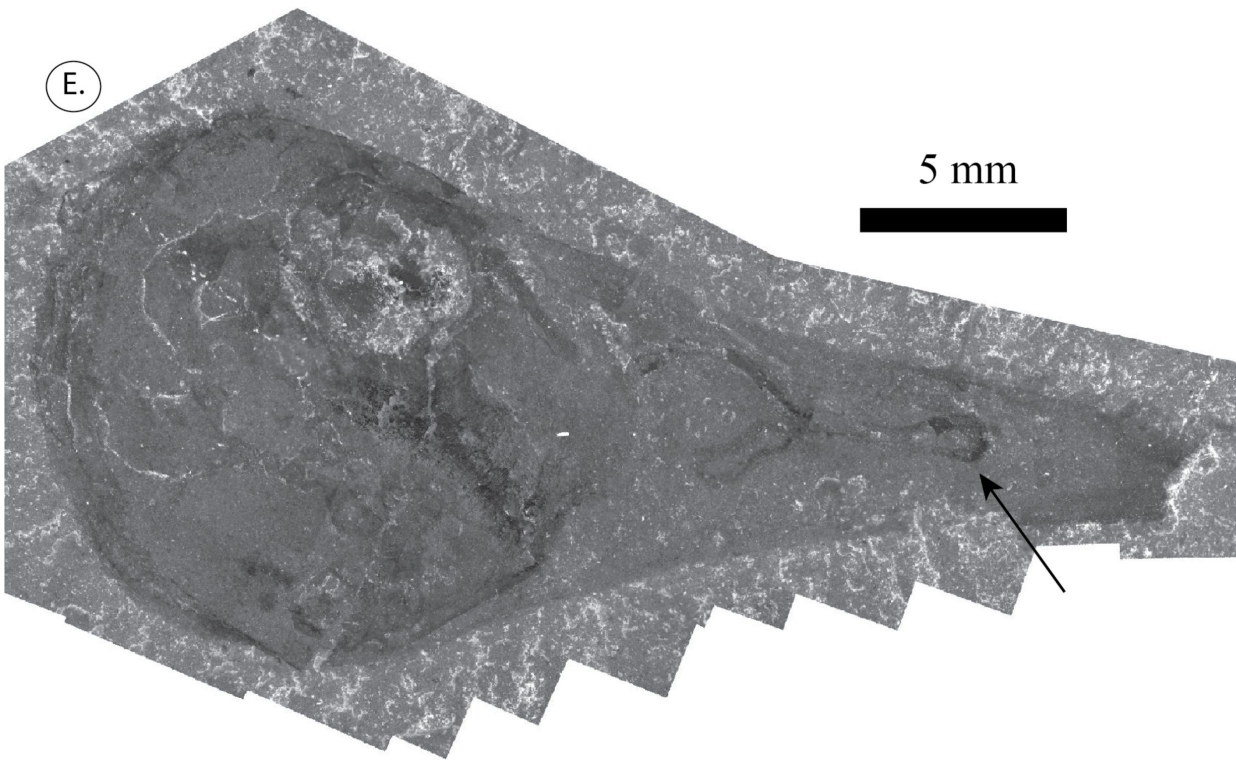
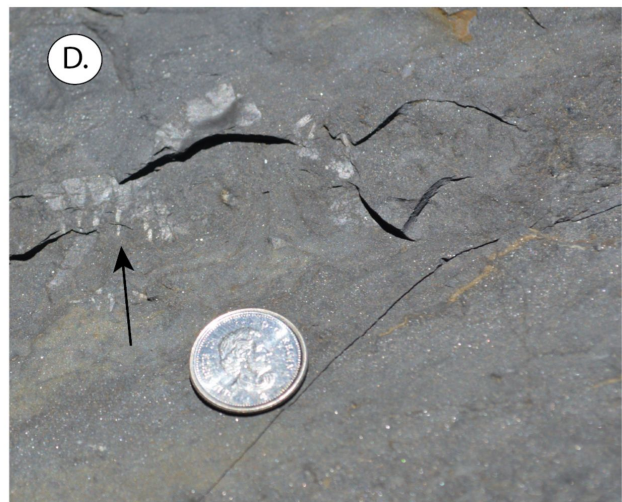
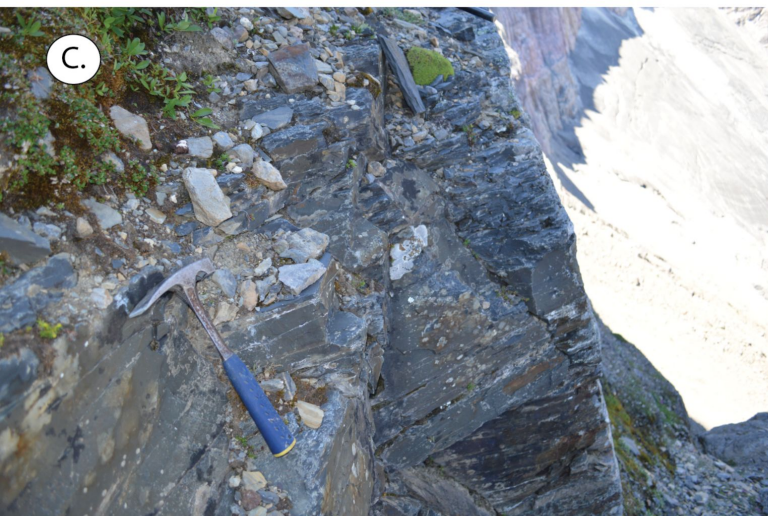
- 616 economic resources of the Cambrian-Ordovician Sauk megasequence of Laurentia. 2012. p.
617 675–723.
- 618 54. Slind OL, Perkins GD. Lower Paleozoic and Proterozoic sediments of the Rocky Mountains
619 between Jasper, Alberta and Pine River, British Columbia. *Bull Can Pet Geol.*
620 1966;14(4):442–68.
- 621 55. McMechan ME. Upper Proterozoic to Middle Cambrian history of the Peace River Arch:
622 evidence from the Rocky Mountains. *Bull Can Pet Geol.* 1990;38(1):36–44.
- 623 56. Bond GC, Christie-Blick N, Kominz MA, Devlin WJ. An early Cambrian rift to post-rift
624 transition in the Cordillera of western North America. *Nature.* 1985;315:742–6.
- 625 57. Lickorish WH, Simony PS. Evidence for late rifting of the Cordilleran margin outlined by
626 stratigraphic division of the Lower Cambrian Gog Group, Rocky Mountain Main Ranges,
627 British Columbia and Alberta. *Can J Earth Sci.* 1995 Jul 1;32(7):860–74.
- 628 58. Fritz WH. Walcott’s lower Cambrian olenellid trilobite collection 61K, Mount Robson area,
629 Canadian Rocky Mountains /. Ottawa, Canada : Geological Survey of Canada,; 1992.
- 630 59. Fritz WH, Mountjoy EW. Lower and early Middle Cambrian formations near Mount
631 Robson, British Columbia and Alberta. *Can J Earth Sci.* 1975;12(2):119–31.
- 632 60. Walcott CD. New Lower Cambrian subfauna. *Smithson Misc Collect.* 1913;57:309–26.
- 633 61. Balthasar U. *Mummpikia* Gen. Nov. and the origin of calcitic-shelled brachiopods.
634 *Palaeontology.* 2008;51:263–79.
- 635 62. Balthasar U. Shell structure, ontogeny and affinities of the Lower Cambrian bivalved
636 problematic fossil *Mickwitzia muralensis*. *Lethaia.* 2004;37:381–400.
- 637 63. Ortega-Hernández J, Esteve J, Butterfield NJ. Humble origins for a successful strategy:
638 complete enrolment in early Cambrian olenellid trilobites. *Biol Lett.* 2013 Oct
639 23;9(5):20130679.
- 640 64. Balthasar U, Butterfield NJ. Early Cambrian “soft-shelled” brachiopods as possible stem-
641 group phoronids. *Acta Palaeontol Pol.* 2009;54:307–14.
- 642 65. Canfield DE, Raiswell R, Westrich JT, Reaves CM, Berner RA. The use of chromium
643 reduction in the analysis of reduced inorganic sulfur in sediments and shale. *Chem Geol.*
644 1986;54:149–55.
- 645 66. Poulton SW, Canfield DE. Development of a sequential extraction procedure for iron:
646 implications for iron partitioning in continentally derived particulates. *Chem Geol.*
647 2005;214:209–21.
- 648 67. Anbar AD, Duan Y, Lyons TW, Arnold GL, Kendall B, Creaser RA, et al. A whiff of
649 oxygen before the Great Oxidation Event? *Science.* 2007;317:1903–6.

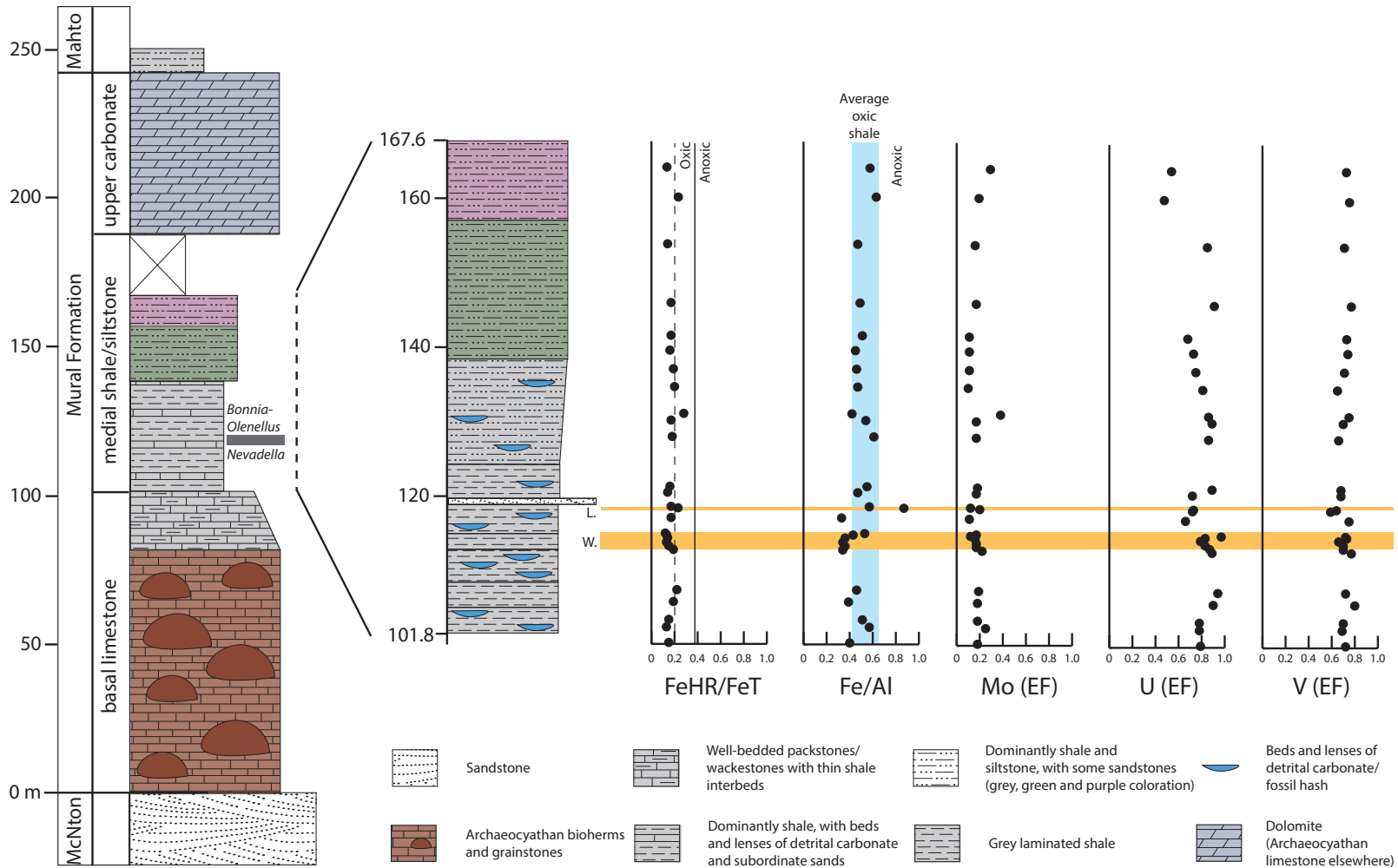
- 650 68. Read PB, Woodsworth GJ, Greenwood HJ, Ghent ED, Evenchick CA. Metamorphic map of
651 the Canadian Cordillera. "A" Series Map 1714A. Geological Survey of Canada; 1991.
- 652 69. Diamond CW, Planavsky NJ, Wang C, Lyons, TW. What the ~1.4 Ga Xiamaling Formation
653 can and cannot tell us about the mid-Proterozoic ocean. *Geobiology*. 2018;16:219–36.
- 654 70. Slotznick SP, Eiler JM, Fischer WW. The effects of metamorphism on iron mineralogy and
655 the iron speciation redox proxy. *Geochim Cosmochim Acta*. 2018 Mar 1;224:96–115.
- 656 71. Lyons TW, Severmann S. A critical look at iron paleoredox proxies: New insights from
657 modern euxinic marine basins. *Geochim Cosmochim Acta*. 2006;70:5698–722.
- 658 72. Raiswell R, Newton R, Bottrell SH, Coburn PM, Briggs DEG, Bond DPG, et al. Turbidite
659 depositional influences on the diagenesis of Beecher's Trilobite Bed and the Hunsrück Slate;
660 sites of soft tissue pyritization. *Am J Sci*. 2008;308(2):105–29.
- 661 73. Paterson JR, García-Bellido DC, Lee MSY, Brock GA, Jago JB, Edgecombe GD. Acute
662 vision in the giant Cambrian predator *Anomalocaris* and the origin of compound eyes.
663 *Nature*. 2011 Dec;480(7376):237–40.
- 664 74. Ma X, Cong P, Hou X, Edgecombe GD, Strausfeld NJ. An exceptionally preserved
665 arthropod cardiovascular system from the early Cambrian. *Nat Commun*. 2014 Apr 7;5:3560.
- 666 75. Ma X, Hou X, Edgecombe GD, Strausfeld NJ. Complex brain and optic lobes in an early
667 Cambrian arthropod. *Nature*. 2012 Oct;490(7419):258–61.
- 668 76. Butterfield NJ. Leangoilia guts and the interpretation of three-dimensional structures in
669 Burgess Shale-type fossils. *Paleobiology*. 2002;28(1):155–71.
- 670 77. Boyer DL, Owens JD, Lyons TW, Droser ML. Joining Forces: Combined Biological and
671 Geochemical Proxies Reveal A Complex but Refined High-Resolution Palaeo-oxygen
672 History in Devonian Epeiric Seas. *Palaeogeogr Palaeoclimatol Palaeoecol*. 2011;306:134–
673 146.
- 674 78. Gaines RR, Droser ML. Paleocology of the familiar trilobite *Elrathia kingii*: An early
675 exaerobic zone inhabitant. *Geology*. 2003;31:941–4.
- 676 79. Garson DE, Gaines RR, Droser ML, Liddell WD, Sappenfield A. Dynamic palaeoredox and
677 exceptional preservation in the Cambrian Spence Shale of Utah. *Lethaia*. 2011;
- 678 80. Ahm A-SC, Bjerrum CJ, Hammarlund EU. Disentangling the record of diagenesis, local
679 redox conditions, and global seawater chemistry during the latest Ordovician glaciation.
680 *Earth Planet Sci Lett*. 2017 Feb 1;459:145–56.
- 681 81. Scott C, Lyons TW. Contrasting molybdenum cycling and isotopic properties in euxinic
682 versus non-euxinic sediments and sedimentary rocks: refining the paleoproxies. *Chem Geol*.
683 2012;324:19–27.

- 684 82. Dahl TW, Ruhl M, Hammarlund EU, Canfield DE, Rosing MT, Bjerrum CJ. Tracing euxinia
685 by molybdenum concentrations in sediments using handheld X-ray fluorescence
686 spectroscopy (HHXRF). *Chem Geol.* 2013;360:241–51.
- 687 83. Gaines RR, Hammarlund EU, Hou X, Qi C, Gabbott SE, Zhao Y, et al. Mechanism for
688 Burgess Shale-type preservation. *Proc Natl Acad Sci.* 2012;109(14):5180–4.
- 689 84. Bergmann KD, Grotzinger JP, Fischer WW. Biological influences on seafloor carbonate
690 precipitation. *PALAIOS.* 2013 Feb 1;28(2):99–115.
- 691 85. Anderson RP, Tosca NJ, Gaines RR, Koch NM, Briggs DEG. A mineralogical signature for
692 Burgess Shale–type fossilization. *Geology.* 2018;
- 693 86. Petrovich R. Mechanisms of Fossilization of the Soft-Bodied and Lightly Armored Faunas of
694 the Burgess Shale and of Some Other Classical Localities. *Am J Sci.* 2001 Oct 1;301(8):683–
695 726.
- 696 87. Wilson LA, Butterfield NJ. Sediment effects on the preservation of Burgess shale–type
697 compression fossils. *PALAIOS.* 2014 Apr 1;29(4):145–54.
- 698 88. McMahon S, Anderson RP, Saupe EE, Briggs DEG. Experimental evidence that clay inhibits
699 bacterial decomposers: Implications for preservation of organic fossils. *Geology.*
700 2016;44:867–70.
- 701 89. Canfield DE. Reactive iron in marine sediments. *Geochim Cosmochim Acta.*
702 1989;53(3):619–32.
- 703 90. Lyons TW, Reinhard CT, Planavsky NJ. The rise of oxygen in Earth’s early ocean and
704 atmosphere. *Nature.* 2014;506(7488):307–15.
- 705 91. Canfield DE, Farquhar J. Animal evolution, bioturbation, and the sulfate evolution of the
706 oceans. *Proc Natl Acad Sci USA.* 2009;106:8123–7.
- 707 92. Lyons TW. A perfect (geochemical) storm yielded exceptional fossils in the early ocean.
708 *Proc Natl Acad Sci.* 2012 Apr 3;109(14):5138–9.
- 709 93. Montjoy EW. *Geology, Mount Robson, West of Sixth Meridian, Alberta-British Columbia.*
710 Geological Survey of Canada; 1980. (“A” Map Series Map 1499A).

711
712







SGP sample_i	Original_num	Height_in_se	Lithology	Fe-carb (wt%	Fe-ox (wt%	Fe-mag (wt%
3321	S1409-100.2	100.2	shale	0.188	0.176	0.122
3322	S1409-102.3	102.3	shale	0.267	0.144	0.145
3323	S1409-103.3	103.3	shale	0.177	0.218	0.186
3324	S1409-105.7	105.7	shale	0.127	0.225	0.097
3325	S1409-107.3	107.3	shale	0.148	0.421	0.165
3326	S1409-112.7	112.7	shale	0.138	0.218	0.098
3327	S1409-113.2	113.2	shale	0.112	0.108	0.123
3328	S1409-113.7	113.7	shale	0.113	0.053	0.151
3329	S1409-114.3	114.3	shale	0.108	0.097	0.173
3330	S1409-114.7	114.7	shale	0.144	0.085	0.18
3331	S1409-114.9	114.9	shale	0.161	0.073	0.179
3332	S1409-117	117	shale	0.102	0.115	0.077
3333	S1409-118.3	118.3	shale	0.241	0.476	0.375
3334	S1409-118.5	118.5	shale	0.21	0.161	0.298
3335	S1409-120.4	120.4	shale	0.166	0.042	0.187
3336	S1409-121.2	121.2	shale	0.248	0.058	0.195
3337	S1409-127.9	127.9	shale	0.499	0.078	0.27
3338	S1409-130.1	130.1	shale	0.339	0.08	0.218
3339	S1409-131	131	shale	0.214	0.174	0.15
3340	S1409-134.6	134.6	shale	0.245	0.095	0.186
3341	S1409-137	137	shale	0.183	0.041	0.156
3342	S1409-139.5	139.5	shale	0.238	0.054	0.224
3343	S1409-141.5	141.5	shale	0.313	0.06	0.277
3344	S1409-145.9	145.9	shale	0.125	0.344	0.237
3345	S1409-153.8	153.8	shale	0.14	0.097	0.16
3346	S1409-160.1	160.1	shale	0.143	0.964	0.218
3347	S1409-164	164	shale	0.117	0.461	0.129
Average				0.19	0.19	0.18
Standard Dev				0.09	0.20	0.07

Fe-py (wt%)	FeT (wt%)	FeHR	FeHR/FeT	Fe-py/FeHR	FeT/Al	TOC (wt%)
0.079	3.82	0.57	0.15	0.14	0.4	0.13
0.089	4.87	0.65	0.13	0.14	0.57	0.13
0.109	4.51	0.69	0.15	0.16	0.51	0.15
0.232	3.5	0.68	0.19	0.34	0.39	0.12
0.128	3.94	0.86	0.22	0.15	0.46	0.18
0.189	3.32	0.64	0.19	0.3	0.34	0.19
0.238	4.03	0.58	0.15	0.41	0.36	0.16
0.185	3.95	0.51	0.13	0.37	0.34	0.16
0.166	4.22	0.55	0.14	0.31	0.36	0.16
0.182	4.54	0.59	0.13	0.31	0.43	0.19
0.216	5.67	0.63	0.12	0.35	0.53	0.22
0.272	3.24	0.56	0.17	0.48	0.33	0.18
0.514	7.46	1.6	0.23	0.32	0.87	0.15
0.284	5.83	0.95	0.17	0.3	0.57	0.13
0.219	4.45	0.62	0.14	0.36	0.47	0.14
0.276	4.97	0.78	0.16	0.36	0.55	0.15
0.185	5.66	1.04	0.18	0.18	0.61	0.13
0.2	5.02	0.84	0.17	0.24	0.54	0.15
0.648	4.22	1.19	0.28	0.55	0.42	0.14
0.47	4.87	1	0.2	0.47	0.47	0.11
0.465	4.58	0.85	0.19	0.55	0.46	0.15
0.211	4.43	0.73	0.16	0.29	0.45	0.12
0.196	4.92	0.85	0.17	0.24	0.51	0.09
0.057	4.63	0.77	0.17	0.08	0.49	0.12
0.234	4.59	0.63	0.14	0.37	0.47	0.1
0.006	5.91	1.34	0.23	0.01	0.62	0.12
0.012	5.43	0.72	0.13	0.01	0.57	0.1
0.22	4.69	0.79	0.17	0.29	0.48	0.14
0.15	0.91	0.26	0.04	0.15	0.11	0.03

Al (wt%)	Ca (wt%)	K (wt%)	Mg (wt%)	Mn (ppm)	Mo (ppm)	Mo EF
9.08	1.27	4.37	1.36	245	0.3	0.18
8.48	4.11	3.8	1.38	629	0.4	0.25
8.85	0.77	4.18	1.36	246	0.3	0.18
8.96	0.09	4.92	0.97	82	0.3	0.18
8.52	0.11	4.16	1.05	105	0.3	0.19
9.64	0.09	5.42	0.81	104	0.4	0.22
9.21	0.07	4.91	1	167	0.3	0.17
9.71	0.14	4.67	1.05	195	0.3	0.17
9.84	0.26	4.66	1.12	255	0.3	0.16
9	0.34	5.13	1.12	265	0.2	0.12
9.2	0.09	4.59	1.21	241	0.3	0.17
9.96	0.07	5.68	0.82	106	0.2	0.11
8	0.47	2.57	1.86	703	0.3	0.2
8.99	0.44	3.42	1.48	479	0.2	0.12
9.51	0.27	4.39	1.09	276	0.3	0.17
9.03	0.4	4.1	1.2	539	0.3	0.18
9.33	0.72	3.92	1.45	1120	0.3	0.17
9.38	0.41	4.45	1.25	911	0.3	0.17
9.97	0.3	5.2	0.86	737	0.7	0.38
10.3	0.3	5.07	1.11	726	0.2	0.1
9.9	0.08	4.82	1.19	556	0.2	0.11
9.89	0.06	4.73	1.14	888	0.2	0.11
9.74	0.15	4.44	1.18	1256	0.2	0.11
9.42	0.08	3.94	0.98	588	0.3	0.17
9.83	0.04	4.23	1.02	266	0.3	0.16
9.55	0.08	2.62	1.16	1295	0.2	0.17
9.57	0.1	2.78	1.11	399	0.3	0.17
9.37	0.42	4.34	1.16	495.52	0.29	0.17
0.53	0.79	0.79	0.22	359.41	0.10	0.06

Na (wt%)	P (ppm)	Th (ppm)	Ti (wt%)	U (ppm)	U EF	V (ppm)	
0.933	470	18.6	0.426	2.5	0.79	87	
0.944	480	16.4	0.374	2.3	0.78	78	
0.945	540	17.7	0.371	2.4	0.78	83	
0.805	370	17.3	0.441	2.8	0.9	95	
0.783	520	19	0.391	2.8	0.94	82	
0.547	540	15.7	0.444	3	0.89	99	
0.639	350	16.3	0.431	2.8	0.87	86	
0.535	540	15.4	0.428	2.8	0.83	90	
0.532	880	17.4	0.407	2.7	0.79	87	
0.523	990	15.3	0.397	2.6	0.83	88	
0.601	340	16.8	0.398	3.1	0.97	88	
0.565	280	16.2	0.455	2.3	0.66	100	
0.987	1430	15	0.309	2	0.72	63	
0.89	1150	20.3	0.429	2.3	0.73	76	
0.818	550	16.7	0.433	2.4	0.72	86	
0.73	730	19.3	0.444	2.8	0.89	82	
0.649	870	17.8	0.432	2.8	0.86	82	
0.556	600	17.2	0.431	2.9	0.89	87	
0.465	590	19.8	0.469	3	0.86	99	
0.403	650	17.9	0.419	2.9	0.81	89	
0.407	230	15.1	0.382	2.6	0.75	93	
0.472	270	16.3	0.426	2.5	0.73	98	
0.81	640	14.2	0.364	2.3	0.68	94	
0.284	330	18.6	0.46	3	0.91	96	
0.337	230	15	0.385	2.9	0.85	93	
0.266	300	12.4	0.362	1.6	0.48	94	
0.277	260	13.1	0.376	1.8	0.54	92	
0.62	560.37	16.70	0.41	2.59	0.79	88.41	
0.22	295.55	1.94	0.04	0.38	0.11	8.21	

V EF	Zn (ppm)	Zr (ppm)
0.72	51	74.7
0.69	60	70.1
0.7	62	68.1
0.8	54	73
0.72	56	81.5
0.77	41	80.2
0.7	58	68.6
0.7	66	68.8
0.66	71	61.1
0.73	70	59.9
0.72	103	59.7
0.75	37	69.8
0.59	124	45.5
0.64	92	60.3
0.68	61	59.9
0.68	80	63.4
0.66	109	55.9
0.7	100	57
0.75	61	70.4
0.65	83	61.8
0.71	93	64.1
0.74	88	72.2
0.73	96	67.9
0.77	73	78.5
0.71	76	75.2
0.74	78	36.3
0.72	68	38.5
0.71	74.48	64.53
0.04	21.04	11.27